MATERIALS SCIENCE

Programmed fluorine binding engineering in anion-pillared metal-organic framework for record trace acetylene capture from ethylene

Xiao-Wen Gu[1]†, Enyu Wu[1]†, Jia-Xin Wang[1], Hui-Min Wen[2], Banglin Chen[3], Bin Li[1]*, Guodong Qian[1]

Porous physisorbents are attractive candidates for selective capture of trace gas or volatile compounds due to their low energy footprints. However, many physisorbents suffer from insufficient sorbate-sorbent interactions, resulting in low uptake or inadequate selectivity when gases are present at trace levels. Here, we report a strategy of programmed fluorine binding engineering in anion-pillared metal-organic frameworks to maximize C_2H_2 binding affinity for benchmark trace C_2H_2 capture from C_2H_4. A robust material (ZJU-300a) was elaborately designed to provide multiple-site fluorine binding model, resulting in an ultrastrong C_2H_2 binding affinity. ZJU-300a exhibits a record-high C_2H_2 uptake of 3.23 millimoles per gram (at 0.01 bar and 296 kelvin) and one of the highest C_2H_2/C_2H_4 selectivity (1672). The adsorption binding of C_2H_2 and C_2H_4 was visualized by gas-loaded ZJU-300a structures. The separation capacity was confirmed by breakthrough experiments for 1/99 C_2H_2/C_2H_4 mixtures, affording the maximal dynamic selectivity (264) and C_2H_4 productivity of 436.7 millimoles per gram.

INTRODUCTION

Selective capture and removal of trace gas or volatile organic compounds represent a major contribution to many environmental and energy consumption issues. For example, during the production of the most critical feedstock ethylene (C_2H_4) through thermal cracking of hydrocarbons, a trace amount of acetylene (C_2H_2) is inevitably coproduced as an impurity (ca. 1%), which would poison the ethylene polymerization catalysts (*1*). Therefore, the removal of trace C_2H_2 impurity from C_2H_4 to an acceptable level [<40 parts per million (ppm)] is of prime importance to obtain polymer-grade ethylene (*2*). Current industrial approaches include catalytic hydrogenation using noble metal catalysts or solvent extraction of cracked olefins by organic solvents; however, they suffer from poor selectivity, high cost, and environment unfriendliness (*3*). Adsorption separation by porous physisorbents has shown to be more attractive than traditional techniques in view of process economy, eco-friendliness, and product purity (*4*–*21*).

Ideal physisorbents should exhibit both high adsorption selectivity and large uptake capacity for trace C_2H_2 component. Owing to the highly designable and tunable pore size and chemistry, a number of microporous metal-organic frameworks (MOFs) have been developed as promising physisorbents for efficient C_2H_2/C_2H_4 separation (*22*–*40*). However, most of the reported materials still suffer from inadequate sorbate-sorbent interactions, leading to low C_2H_2 uptake or insufficient selectivity when C_2H_2 gas is present at trace concentrations. Among them, anion-pillared SIFSIX materials represent the most promising subclass of MOF adsorbents, which consist of square lattice layers of organic ligands and metal nodes, pillared by fluorinated anions to generate a three-dimensional (3D) network with primitive cubic (pcu) topology (*41*–*49*). SIFSIX materials with pcu topology are typically divided into two categories: non-interpenetration and twofold interpenetration. The non-interpenetrated materials (e.g., SIFSIX-1-Cu and SIFSIX-3, classified into the first generation) show the preferential binding of C_2H_2 over C_2H_4 because the fluorinated anions have a stronger interaction with C_2H_2. However, these materials exhibit the relatively large pore sizes (>4.2 Å) and insufficient C_2H_2 binding affinity with a moderate adsorption enthalpy (Q_{st}) of ca. 30 kJ mol^{-1}, delimiting their C_2H_2/C_2H_4 selectivity less than 10 (*47*). To further improve gas selectivity, the interpenetration strategy was used to fine-tune pore size/chemistry in SIFSIX platform. Some twofold interpenetrated SIFSIX materials (classified into the second generation) were developed to boost C_2H_2/C_2H_4 separation (*47*, *48*). Such interpenetration architecture was found to enable each C_2H_2 molecule to simultaneously bind with two F atoms from different nets through C—H···F hydrogen bonding (Fig. 1), leading to much stronger C_2H_2 binding energy (ca. 40 kJ mol^{-1}) than the first-generation materials. For example, SIFSIX-2-Cu-i with aperture size of 4.4 Å exhibits both improved uptake capacity and gas selectivity (*44*) for trace C_2H_2 component (*47*). Fine-tuning of pore size to 3.4 Å in SIFSIX-14-Cu-i (also called UTSA-200a) resulted in the nearly molecular sieving of C_2H_2 from C_2H_4 with the record selectivity up to 6000 (*48*), surpassing all the previous benchmark materials. However, the two-site fluorine binding model of the second-generation materials limited their trace C_2H_2 uptake not so high (1.5 to 1.8 mmol g^{-1} at 0.01 bar) due to the inadequate binding energy. Furthermore, the stability investigations of SIFSIX-14-Cu-i in a moist environment revealed a structural phase change, which resulted in the loss of C_2H_2 capture and thus precluded the practical applications (*48*). Therefore, the state-of-the-art SIFSIX materials still suffer from the insufficient low-pressure C_2H_2 uptake and poor moisture stability, and there is a lack of ideal and stable materials to have both ultrahigh C_2H_2 uptake and selectivity for trace C_2H_2 removal from C_2H_4.

[1]State Key Laboratory of Silicon and Advanced Semiconductor Materials, School of Materials Science and Engineering, Zhejiang University, Hangzhou 310027, China. [2]College of Chemical Engineering, Zhejiang University of Technology, Hangzhou 310014, China. [3]Fujian Provincial Key Laboratory of Polymer Materials, College of Chemistry and Materials Science, Fujian Normal University, Fuzhou 350007, China.
*Corresponding author. Email: bin.li@zju.edu.cn
†These authors contributed equally to this work.

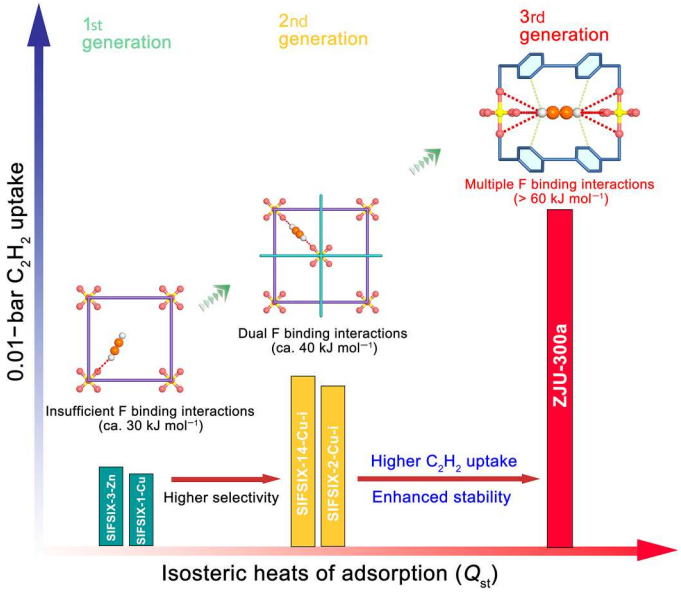

Fig. 1. Programmed fluorine binding engineering in anion-pillared SIFSIX materials for C_2H_2/C_2H_4 separation, indicating the proposed strategy of designing multiple fluorine binding interactions to target both ultrahigh C_2H_2 capture and selectivity.

To address the above drawbacks, we sought to develop a new generation of robust SIFSIX material that affords a superior C_2H_2 uptake capacity at 0.01 bar while maintaining the record-high gas selectivity. As we know, when gas selectivity reaches a very high level, the separation performance for 1/99 C_2H_2/C_2H_4 mixtures would be mainly dominated by trace C_2H_2 uptake at 0.01 bar (*40*, *48*). To maximize the low-pressure C_2H_2 uptake capacity, it is important to construct stronger binding sites in SIFSIX materials than that in the second generation. However, SIFSIX materials with pcu topology have shown the limitation to achieve the above targets due to the insufficient fluorine binding model. We envisioned that, if we can construct a unique type of multiple-site fluorine binding model that enables more fluorine atoms to simultaneously interact with C_2H_2 (Fig. 1), then it is highly potential to maximize C_2H_2 binding affinity and thus boost trace C_2H_2 removal for C_2H_4 purification. By programmed fluorine binding engineering, we here designed and synthesized a stable SIFSIX material, $[Zn(TPE)SiF_6]_n$ [termed as ZJU-300, 1,1,2,2-tetra(pyridin-4-yl)ethene (TPE)]. This material features a non-interpenetrated framework with fsc (four, six type c) topology (*50*) and appropriate channel pore aperture size of 3.8 Å (Fig. 2). Such structural architecture enables SiF_6^{2-} anions to be parallelly adjacent in close proximity with a F···F distance of 3.8 Å, offering the proposed multiple-site fluorine binding model for trace C_2H_2 capture. Single-crystal x-ray diffraction (SCXRD) experiments on gas-loaded ZJU-300a visually unveiled that such multiple-site fluorine binding model allows eight fluorine atoms to concurrently and strongly interact with C_2H_2 molecule, resulting in an ultrastrong C_2H_2 binding affinity with the highest Q_{st} value (61.1 kJ mol^{-1}) among SIFSIX materials. The activated ZJU-300a thus exhibits the record-high C_2H_2 uptake of 3.23 mmol g^{-1} (at 0.01 bar and 296 K) and one of the highest C_2H_2/C_2H_4 selectivity (1672), setting up a benchmark for this separation. Dynamic breakthrough experiments on 1/99 C_2H_2/C_2H_4 mixtures provide both record-high dynamic separation selectivity (264) and C_2H_4 purification capacity of 436.7 mmol g^{-1}, several times higher than the reported state-of-the-art SIFSIX-14-Cu-i (91 and 101.3 mmol g^{-1}) (*48*) and zeolite Ni@faujasite (Ni@FAU) (97 and 116.8 mmol g^{-1}) (*32*).

RESULTS

Synthesis and characterization

The organic ligand of TPE was simply synthesized through a multistep reaction procedure (fig. S1). The slow diffusion of a methanol solution of $ZnSiF_6{\cdot}6H_2O$ into a TPE solution for 1 week produced ZJU-300 as colorless block crystals suitable for single-crystal x-ray analysis. The powder samples can be facilely produced by an alternative fast mixing method. A methanol solution (5 ml) of $ZnSiF_6{\cdot}6H_2O$ (0.125 mmol) was added to a methanol solution (15 ml) of TPE (0.15 mmol) at 80°C, and the mixtures were kept at 80°C for as short as 10 min to obtain a white powder. This facile synthesis indicates its potential to be produced at large scale. The purity of the bulk sample was confirmed by powder x-ray diffraction patterns (PXRDs) and gas adsorption measurements (fig. S3). Scanning electron microscopy (SEM) images revealed that the single crystals and rapidly synthesized particles of ZJU-300 show the same cubic morphology but with different dimensions (fig. S4).

The SCXRD studies indicated that the framework of ZJU-300 crystallizes in a tetragonal *P*4/*mcc* space group (No. 124). As depicted in Fig. 2 (A and B), the use of different types of organic linkers to construct SIFSIX materials could result in different structure network and pore characteristic. In general, the first- and second-generation SIFSIX materials are built from two-connected N-donor ligands to construct the pcu topology and square pores (*41*–*49*). However, the use of four-connected organic linkers can lead to a different structure topology (*51*–*53*). As shown in Fig. 2C, four terminal nitrogen atoms of TPE linkers coordinate with zinc(II) atoms to construct a 2D $[Zn(TPE)]_n$ layer. The 2D layers are further pillared by SiF_6^{2-} anions in the third dimension to form a 3D network without interpenetration. Unlike the pcu topology in square grid SIFSIX materials, the resulting ZJU-300 holds a 4,6-connected fsc network (Fig. 2B). ZJU-300 exhibits two types of small rhombic pore channels with the same window size of 3.8 Å by 3.1 Å, viewed along the *c* axis. In addition, another type of pore channels with the aperture size of 3.8 Å by 2.7 Å was observed along the *a* and *b* axes. The aperture sizes of all the pore channels are larger than the kinetic diameter of C_2H_2 (3.3 Å) but smaller than that of C_2H_4 (4.2 Å). Because of the non-interpenetration feature, the SiF_6^{2-} anions in ZJU-300 are parallelly adjacent and in close proximity to each other in the same layer, with a short F···F distance of 3.8 Å after subtracting van der Waals radius. Such adjacent SiF_6^{2-} anions combined with TPE linkers can form three types of pore cavities with small size of 3.8 Å. In each cavity, eight F atoms from adjacent SiF_6^{2-} anions point toward the center of the cavity with the average distance of 3.2 and 4.0 Å between these F atoms and center of the cavity, which creates multiple-site fluorine binding model to provide very strong adsorption sites for C_2H_2 capture. In comparison, the SiF_6^{2-} anions in the benchmark SIFSIX-14-Cu-i are stagger disposed along pore channels due to the twofold interpenetration, restricting only two F atoms to interact with C_2H_2 molecule (fig. S16) (*48*). Evidently, the unique multiple fluorine binding sites observed in ZJU-300 enable more F atoms to

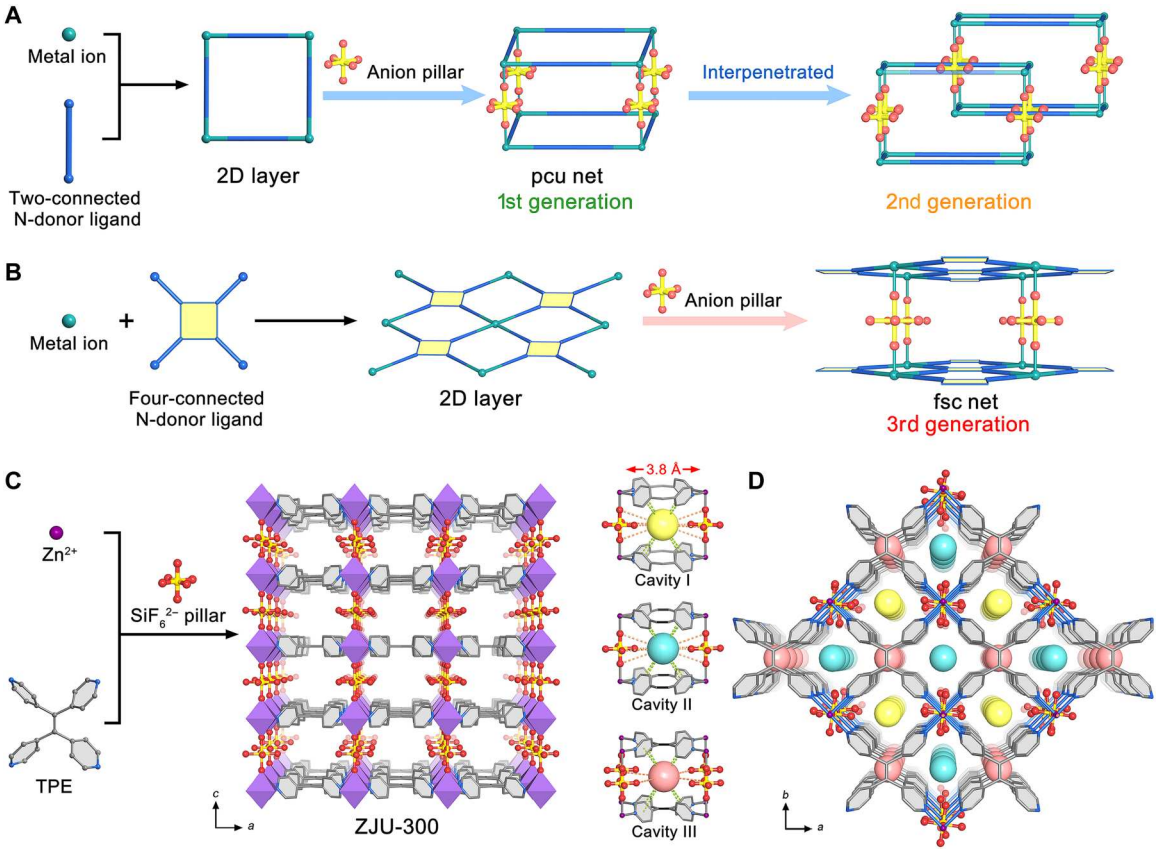

Fig. 2. Description of the crystal structure of ZJU-300. (**A**) Scheme illustration of the first-generation and second-generation SIFSIX materials with pcu topology. (**B**) Scheme illustration of a type of SIFSIX materials, built from four-connected N-donor ligands to construct the fsc topology and rhombic pores containing parallelly adjacent SiF_6^{2-} anions. (**C**) Single-crystal structure of ZJU-300 viewed along with the *b* axis, exhibiting three types of pore cavities served as potential C_2H_2 binding sites (H atoms have been omitted for clarity). (**D**) The staggered arrangement feature of pore cavities. Color code: Zn (purple), Si (yellow), F (red), N (blue), and C (gray).

interact with C_2H_2 compared to SIFSIX-14-Cu-i, probably leading to much stronger C_2H_2 adsorption affinity. Furthermore, there exist a large amount of pore cavities densely and orderly arranged in ZJU-300, in which cavity I and cavity III are staggered with each other along the *b* axis, and cavity II and cavity III show a staggered arrangement along the *a* axis (Fig. 2D). Therefore, the dense pore cavities with multiple fluorine binding sites not only can provide an ultrastrong binding affinity for trace C_2H_2 capture but also can enable the dense packing of C_2H_2 molecules within the pores, potentially affording both ultrahigh C_2H_2 capture capacity and selectivity for trace C_2H_2 removal.

The permanent porosity of activated ZJU-300a was determined by nitrogen (N_2) sorption isotherms at 77 K. As revealed in Fig. 3A, ZJU-300a exhibits a typical type I sorption behavior, and the saturated N_2 uptake is up to 244 $cm^3\ g^{-1}$. The Brunauer-Emmett-Teller surface area and pore volume of ZJU-300a were calculated to be 796.2 $m^2\ g^{-1}$ and 0.38 $cm^3\ g^{-1}$, respectively, which are 30.1 and 40.7% higher than those of SIFSIX-14-Cu-i (612.0 $m^2\ g^{-1}$ and 0.27 $cm^3\ g^{-1}$) (fig. S5) (*48*). Such larger surface area/pore volume observed in ZJU-300a can provide more pore spaces to capture more C_2H_2 molecules and thus improve C_2H_2 adsorption amount. The pore size distribution, determined by the Horvath-Kawazoe model based on N_2 adsorption at 77 K, shows a pore size of 4.1 Å (Fig. 3A), close to the result observed from the crystal structure.

Gas adsorption measurements

Single-component adsorption isotherms of ZJU-300a for C_2H_2 and C_2H_4 were collected at different temperatures up to 1 bar (Fig. 3B and figs. S6 to S8), respectively. As presented in Fig. 3 (B and C), ZJU-300a exhibits an extremely steep C_2H_2 adsorption increase at the low-pressure region and 296 K, much faster than that of the first- and second-generation materials (e.g., SIFSIX-1-Cu, SIFSIX-14-Cu-i, and SIFSIX-2-Cu-i). This indicates that ZJU-300a shows a much stronger binding affinity toward C_2H_2. At a partial pressure of 0.01 bar, as an indicator of the C_2H_2 capture ability of adsorbents from 1/99 C_2H_2/C_2H_4 mixture, ZJU-300a shows a record-high C_2H_2 uptake amount of 3.23 mmol g^{-1}, which is substantially higher than all the SIFSIX materials and almost two times higher than that of the benchmark SIFSIX-14-Cu-i (1.83 mmol g^{-1}) (*48*). As shown in Fig. 3D, this C_2H_2 uptake at 0.01 bar notably surpasses the other state-of-the-art materials reported so far, including Ni@FAU (1.72 mmol g^{-1}) (*32*), Cu(4,4′-dipyridylsulfone)$_2$(TiF_6) (ZUL-100) (2.96 mmol g^{-1}) (*40*), and Cu_2(1,3,5,7-adaman-tane tetracarboxylic acid) (ATC-Cu) (2.54 mmol g^{-1}) (*54*). Under 296 K and 1 bar, the C_2H_2 uptake of ZJU-300a gradually increases to 5.37 mmol g^{-1}, which is also much higher than that of SIFSIX-

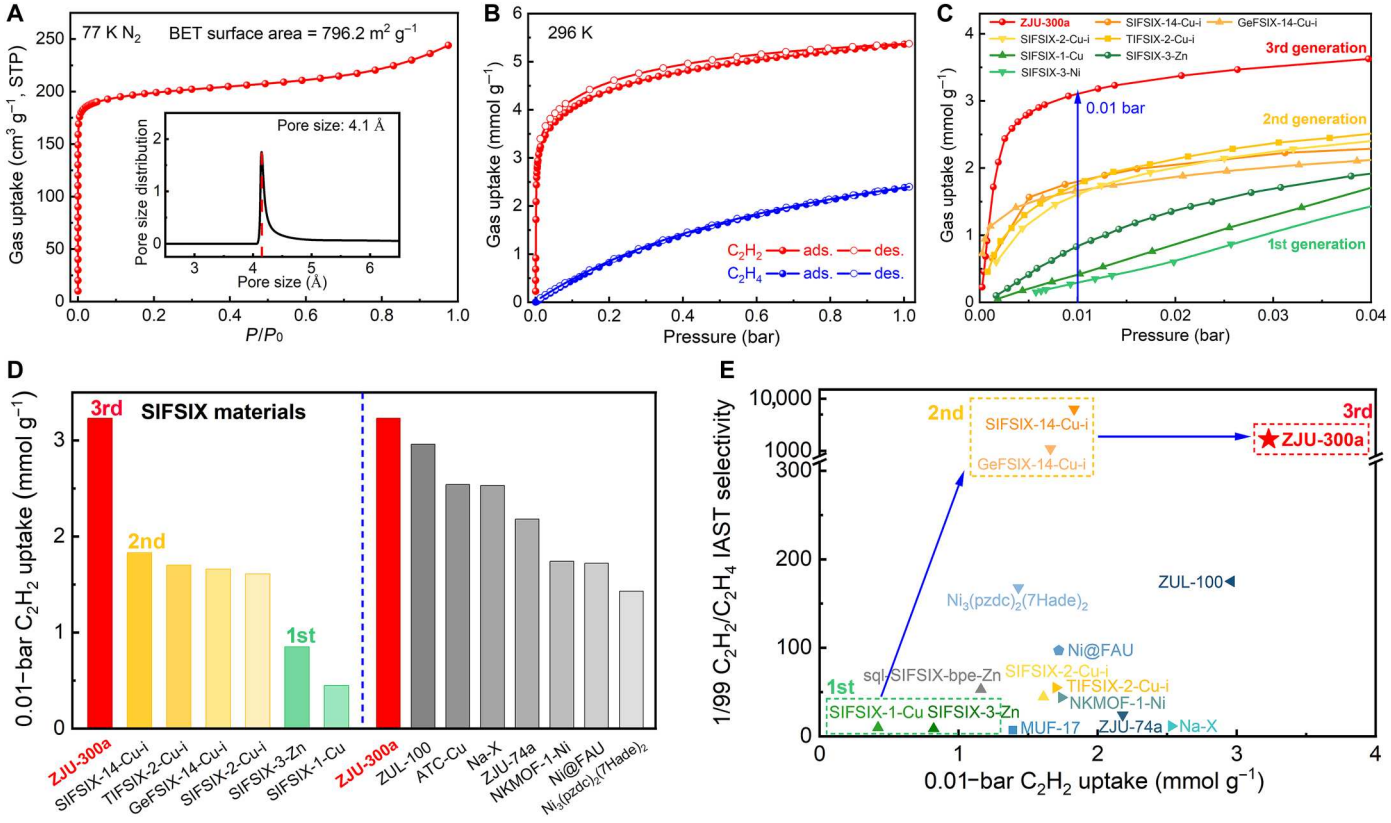

Fig. 3. Gas sorption properties. (**A**) N_2 adsorption isotherm of ZJU-300a at 77 K. Inset shows pore size distribution for ZJU-300a based on Horvath-Kawazoe model. BET, Brunauer-Emmett-Teller. STP, standard temperature and pressure. P/P_0, the ratio of actual preesure to saturated vapor pressure. (**B**) Adsorption isotherms of ZJU-300a for C_2H_2 (red) and C_2H_4 (blue) at 296 K. (ads, adsorption; des, desorption). (**C**) Comparison of C_2H_2 uptake (0 to 0.04 bar) among the representative SIFSIX materials at room temperature. (**D**) Comparison of C_2H_2 capture capacity for ZJU-300a with SIFSIX materials and other best-performing materials at 0.01 bar. (**E**) Comparison of C_2H_2 uptake at 0.01 bar and 1/99 C_2H_2/C_2H_4 selectivity for ZJU-300a with the top-performing materials reported.

14-Cu-i (3.65 mmol g^{-1}) due to its increased surface area (fig. S9) (*48*). Compared with C_2H_2 adsorption, the C_2H_4 uptake in ZJU-300a increases much slowly in the whole pressure ranges with a much lower uptake of 2.39 mmol g^{-1} at 296 K and 1 bar (Fig. 3B), affording an obviously preferential adsorption of C_2H_2 over C_2H_4. This large adsorption difference between C_2H_2 and C_2H_4 can be well supported by the experimental isosteric heat of adsorption (Q_{st}), wherein the initial Q_{st} value of C_2H_2 (61.1 kJ mol^{-1}) is notably higher than that of C_2H_4 (39.7 kJ mol^{-1}) found in ZJU-300a (fig. S10). The C_2H_2 Q_{st} value of ZJU-300a is also higher than that of SIFSIX-1-Cu (30.0 kJ mol^{-1}) (*47*), SIFSIX-3-Zn (21.0 kJ mol^{-1}) (*47*), and SIFSIX-14-Cu-i (40.0 kJ mol^{-1}) (*48*), further confirming its strongest C_2H_2 binding affinity among SIFSIX materials (fig. S13). In addition, we also investigated the time-dependent adsorption kinetics profiles of rapidly synthesized ZJU-300a at 296 K. As shown in fig. S14, ZJU-300a shows a notably faster initial rate for C_2H_2 adsorption than C_2H_4, and both gas adsorption reaches equilibrium rapidly within 10 min. Fitting the adsorption data with micropore diffusion model (*55*) affords a high kinetic selectivity of 19.2, which can further promote its high separation performance for C_2H_2/C_2H_4 mixtures.

Next, we used ideal adsorbed solution theory (IAST) to calculate the adsorption selectivity of ZJU-300a for 1/99 C_2H_2/C_2H_4 mixture (*56*). As shown in fig. S15, owing to the record-high C_2H_2 capture capacity at 0.01 bar and low C_2H_4 uptake, ZJU-300a exhibits one of the highest IAST selectivity of 1672 at 296 K and 1 bar, far surpassing that of the first- and second-generation SIFSIX materials except SIFSIX-14-Cu-i (Fig. 3E). We note that this selectivity is also notably higher than the other benchmark materials, such as Ni@FAU (97) (*32*), ZUL-100 (175) (*40*), and $Ni_3(pzdc)_2(7Hade)_2$ (168) (*31*). As we know, adsorption selectivity and uptake capacity have been deemed as the two most important criteria to evaluate the separation performance of adsorbents. As shown in Fig. 3E, the first-generation SIFSIX materials show both low C_2H_2 uptake at 0.01 bar and poor gas selectivity due to their relatively large pore size and insufficient binding affinity. Fine-tuning of pore size and interpenetration in the second-generation leads to both notably enhanced C_2H_2 uptake and selectivity, wherein the representative SIFSIX-14-Cu-i exhibits the record gas selectivity (*48*). By optimizing the ultrastrong multiple-site fluorine binding model, ZJU-300a displays the markedly improved C_2H_2 uptake (3.23 versus 1.83 mmol g^{-1}) while maintaining the comparably high selectivity in comparison to SIFSIX-14-Cu-i (Fig. 3E). When compared with other best-performing materials, ZJU-300a also achieves both the highest C_2H_2 uptake capacity and gas selectivity so far, making it as the current benchmark for C_2H_2/C_2H_4 separation.

Single-crystal diffraction studies on gas-loaded ZJU-300a

To gain better insight into the record C_2H_2 capture capacity and selectivity of ZJU-300a, we performed the SCXRD experiments on both C_2H_2- and C_2H_4-loaded ZJU-300a crystals to directly visualize the locations of the adsorbed C_2H_2 and C_2H_4 molecules. According to the SCXRD analysis, C_2H_2@ZJU-300a was found to exhibit three types of binding sites (site 1, site 2, and site 3) for C_2H_2 molecules (Fig. 4, A and B), which are preferentially located at two rhombic pore channels (cavity I and cavity II in Fig. 2) and at the middle of two adjacent TPE ligands (cavity III). As shown in Fig. 4 (C and D), the adsorbed C_2H_2 molecules on site 1 and site 2 exhibit the same binding interactions with the host framework. Each C_2H_2 molecule at these two sites strongly interacts with eight F atoms originated from two adjacent SiF_6^{2-} anions through cooperative eight C—H···F hydrogen bonds, with the distances of 2.11 to 3.84 Å. Furthermore, the C_2H_2 molecule is also bound with eight C—H groups from four surrounding pyridine rings of TPE linkers through supramolecular interactions (C_{C2H2}···H = 3.03 to 3.36 Å). The site 3 C_2H_2 molecule located at the middle of two adjacent TPE ligands surrounded by four SiF_6^{2-} anions (Fig. 4E). Similarly, each C_2H_2 molecule at this site is cooperatively bound with two SiF_6^{2-} anions through two C—H···F hydrogen bonding and with eight pyridine rings of TPE linkers through eight supramolecular interactions (C_{C2H2}···H = 2.84 to 3.33 Å). In comparison, the two-interpenetrated SIFSIX materials (e.g., SIFSIX-14-Cu-i) have been revealed to show one type of binding sites, in which each C_2H_2 molecule can interact with two SiF_6^{2-} sites from different nets through two C—H···F hydrogen bonds (fig. S16) (*48*). Evidently, the non-interpenetration framework with fsc topology in ZJU-300a can create a unique multiple fluorine binding site to offer more numbers of C—H···F hydrogen bonds and additional supramolecular interactions with C_2H_2, thus resulting in the much stronger C_2H_2 binding affinity. Furthermore, because of the dense distribution of these three binding sites, the site 1 adsorbed C_2H_2 interacts with two adjacent C_2H_2 molecules in site 3 through the C—H···C interactions (2.71 and 3.84 Å), forming the interlaced C_2H_2 chains within the channels along the *b* axis (Fig. 4A). Similarly, each C_2H_2 molecule in site 2 is also bounded to two site 3 C_2H_2 molecules (4.33 and 4.35 Å) along the *a* axis. Therefore, the dense and strong multiple fluorine binding sites observed in ZJU-300a not only provide the ultrastrong binding affinity for C_2H_2 capture but also enable the dense packing of C_2H_2 within the pores, thus contributing to its record-high uptake capacity at 0.01 bar. The SCXRD data indicate that the adsorbed C_2H_2 amount in site 1, site 2, and site 3 corresponds to 1.84, 1.84, and 1.84 mmol g^{-1} gas uptake (fig. S17 and more detailed explanation in the Supplementary Materials), and the total value of 5.52 mmol g^{-1} is very close to the experimental C_2H_2 uptake (5.37 mmol g^{-1}) at 296 K and 1 bar.

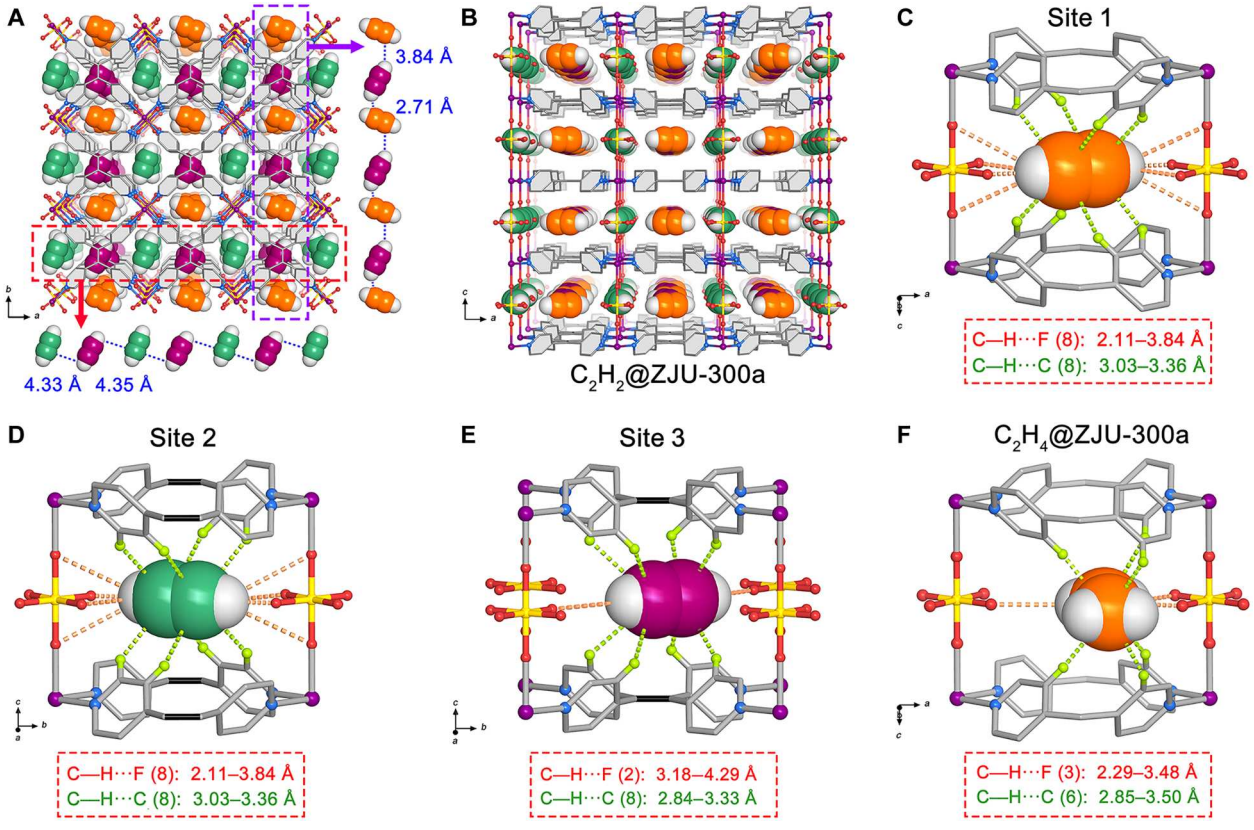

Fig. 4. Adsorption binding sites of C_2H_2 and C_2H_4 in ZJU-300a. (**A**) The SCXRD structure of C_2H_2-loaded ZJU-300a viewed along the *c* axis, indicating three types of binding sites for C_2H_2 and the intermolecular interactions between the adsorbed C_2H_2 molecules. (**B**) The dense packing of C_2H_2 in the whole structure of ZJU-300a, viewed along the *b* axis. (**C**) Illustration of the binding interactions of C_2H_2 molecules in ZJU-300a at site 1, (**D**) site 2, and (**E**) site 3, as determined by SCXRD studies. (**F**) Illustration of the binding interactions of C_2H_4 molecule in ZJU-300a obtained by SCXRD studies.

In contrast, the crystal structure of C_2H_4@ZJU-300a revealed that the adsorbed C_2H_4 molecules show one type of binding sites, primarily located at the corner of the rhombic pore channels (fig. S18). As shown in Fig. 4F, each C_2H_4 molecule can interact with two SiF_6^{2-} anions through three C—H···F hydrogen bonding (2.29 to 3.48 Å) and with six pyridine rings of TPE linkers through supramolecular interactions (C_{C2H2}···H = 2.85 to 3.50 Å). Compared with that of C_2H_2, C_2H_4 molecule shows a much weaker interaction with the framework because of its much less and weaker C—H···F hydrogen bonds. This can be further confirmed by the higher experimental Q_{st} value of C_2H_2 (61.1 kJ mol^{-1}) than that of C_2H_4 (39.7 kJ mol^{-1}). Thus, the more number of binding sites and much higher binding affinity toward C_2H_2 afford the ultrahigh C_2H_2/C_2H_4 selectivity of ZJU-300a. All of these results can visually elucidate the mechanisms of both ultrahigh C_2H_2 adsorption and selectivity observed in ZJU-300a.

Column breakthrough experiments

To validate the excellent separation performance of ZJU-300a for actual 1/99 C_2H_2/C_2H_4 mixtures, the dynamic breakthrough experiments were conducted on a packed column of activated ZJU-300a at 296 K under a total gas flow of 5 ml min^{-1}. For a comparison, the breakthrough experiments on the fixed bed adsorbers packed with the first-generation SIFSIX-1-Cu and the second-generation SIFSIX-14-Cu-i were also measured under the same conditions. The experimental breakthrough curves for all the selected SIFSIX materials are depicted in Fig. 5A. Efficient separation can be accomplished by all these materials for 1/99 C_2H_2/C_2H_4 mixtures. The C_2H_2 breakthrough time was observed to be 128 and 512 min g^{-1} for SIFSIX-1-Cu and SIFSIX-14-Cu-i, affording a polymer-grade C_2H_4 productivity of 20.6 and 101.3 mmol g^{-1}, respectively. These C_2H_4 productivities are slightly higher than the values reported in the literatures (17.7 and 85.7 mmol g^{-1} for SIFSIX-1-Cu and SIFSIX-14-Cu-i) (*47*, *48*). Similarly, a highly efficient separation for C_2H_2/C_2H_4 mixture was also achieved by ZJU-300a: The C_2H_4 gas eluted through the adsorption bed immediately in a high-purity grade, whereas C_2H_2 was retained in the packed column over 2058 min g^{-1}. This C_2H_2 breakthrough time of ZJU-300a is even 4.1 times longer than that observed in SIFSIX-14-Cu-i. According to the breakthrough curves, the C_2H_2/C_2H_4 dynamic selectivity of ZJU-300a was calculated to be 264 (Fig. 5C and fig. S19), notably higher than all the reported materials including the previous state-of-the-art Ni@FAU (97) (*32*) and SIFSIX-14-Cu-i (91). During the breakthrough process, ultrapure C_2H_4 (C_2H_2 < 1 ppm) productivity from the outlet effluent for ZJU-300a was determined to be record high of 436.7 mmol g^{-1}. As revealed in Fig. 5B, this polymer-grade C_2H_4 productivity far surpasses all the SIFSIX materials, including four times larger than SIFSIX-14-Cu-i (101.3 mmol g^{-1}). Note that, although ZJU-300a shows a slightly lower IAST selectivity than SIFSIX-14-Cu-i, the much higher C_2H_2

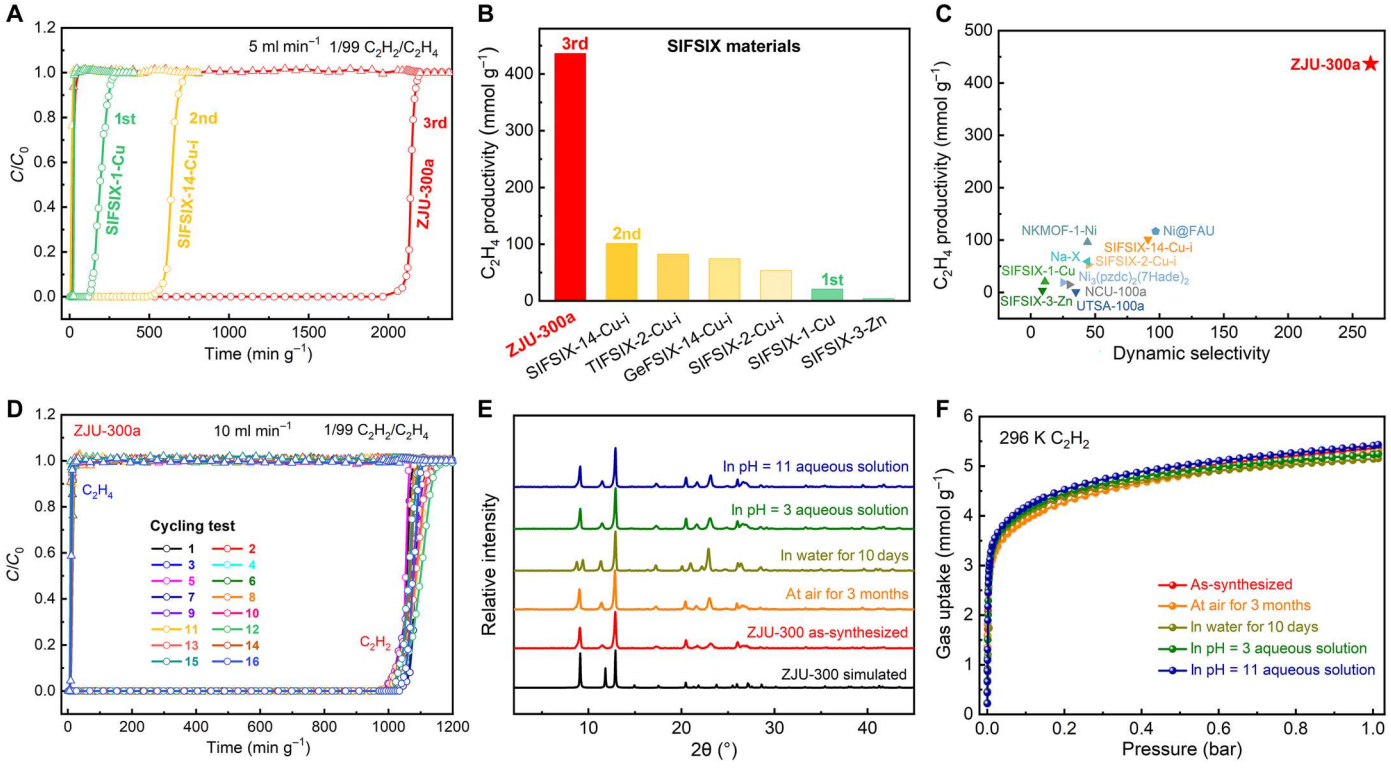

Fig. 5. Breakthrough experiments and stability characterization. (**A**) Experimental column breakthrough curves for 1/99 C_2H_2/C_2H_4 separation with ZJU-300a, SIFSIX-14-Cu-i, and SIFSIX-1-Cu at a flow rate of 5 ml min^{-1} under ambient conditions, respectively. (**B**) Comparison of experimental C_2H_4 productivity from C_2H_2/C_2H_4 (1/99) mixture through fixed bed adsorbers packed with ZJU-300a and representative SIFSIX materials. (**C**) Comparison of C_2H_4 productivity and dynamic selectivity of ZJU-300a with other top-performing materials, obtained from the breakthrough curves. (**D**) The cycling tests of 1/99 C_2H_2/C_2H_4 mixture with a flow rate of 10 ml min^{-1} in an absorber bed packed with ZJU-300a under ambient conditions. C/C_0, the ratio of gas concentration at the outlet and inlet. (**E**) PXRD patterns of ZJU-300 samples after treatment under different conditions. (**F**) C_2H_2 adsorption isotherms at 296 K treated under various conditions.

uptake at 0.01 bar (3.23 versus 1.83 mmol g^{-1}) led to its four times higher C_2H_4 productivity in breakthrough experiments. This result verifies that, when gas selectivity reaches a very high level, C_2H_2 uptake capacity at 0.01 bar would play the most important role to determine the final C_2H_4 productivity. When compared with the other best-performing materials, ZJU-300a also shows the highest C_2H_4 productivity (Fig. 5C), much larger than that of ZUL-100 (134.1 mmol g^{-1}) (*40*) and Ni@FAU (116.8 mmol g^{-1}) (*32*). Subsequently, multiple breakthrough experiments on C_2H_2/C_2H_4 mixed gas indicate that the separation capacity of ZJU-300a can be recycled at least 15 continuous cycles (Fig. 5D), confirming its feasible recyclability and regeneration capability. As inferred from the PXRD and gas adsorption studies on associated samples, ZJU-300a can maintain its structural integrity after multiple breakthrough experiments (figs. S20 to S22).

Stability characterization

Given that the feed gases in the practical C_2H_2 removal unit often contain a small amount of water and acidic gases (*57*), the extreme separation conditions require adsorbents with high and long-term water and pH stability. Unfortunately, most of square grid SIFSIX materials with pcu topology were observed to decompose or undergo phase transformations under low levels of water and moisture conditions (*58*). As shown in figs. S23 to S28 and table S5, our PXRD experiments confirmed that the crystallinity of most representative SIFSIX materials (e.g., SIFSIX-1-Cu, SIFSIX-2-Cu-i, and SIFSIX-14-Cu-i) was lost after exposure to the moisture or water solution, severely dampening their industrial applications. However, ZJU-300 with fsc topology exhibits an extremely high and long-term stability toward water and acid-base environments. As depicted in Fig. 5E, the framework of ZJU-300 can retain its structural integrity without phase change or loss of crystallinity observed after exposed to air for 3 months or water for 10 days, as revealed by PXRD patterns. Furthermore, the ZJU-300 samples were immersed in HCl (pH 3) and NaOH (pH 11) solutions for 1 day, respectively. The PXRD patterns indicate that the framework also can maintain structural stability with no phase transformation observed. The C_2H_2 uptake capacities at 296 K after the above treatments are very close to those of the pristine material (Fig. 5F), further confirming its ultrahigh chemical stability. Variable temperature PXRD patterns revealed that ZJU-300 shows a high thermal stability up to 200°C (fig. S30). The high stability encouraged us to further evaluate its separation performance for a 1/99 C_2H_2/C_2H_4 mixture under 40% humidity conditions. As shown in fig. S31, ZJU-300a can almost retain its exceptional separation capacity with slightly decreased dynamic selectivity (252) and C_2H_4 productivity (430.3 mmol g^{-1}), indicating that the presence of water vapor has a slight effect on the separation capacity. Given that the feed streams in industry typically contain a small amount of acidic gas (e.g., H_2S) (*59*), the breakthrough experiments for a 1/99 mixture with 1000 ppm H_2S were also performed on ZJU-300a to investigate the effect of acidic gases. As shown in fig. S32, the largely overlapped breakthrough curves reveal that ZJU-300a can retain its high separation capacity under this condition. Overall, compared with the previously best SIFSIX-14-Cu-i, ZJU-300 exhibits both the substantially improved 0.01-bar C_2H_2 capture capacity and water/pH stability while maintaining the ultrahigh gas selectivity, making it as the current benchmark for the important C_2H_2/C_2H_4 separation. In comparison to the state-of-the-art zeolites (e.g., Ni@FAU and Na-X) (*32*, *35*), although ZJU-300a holds some superiorities in gravimetric C_2H_2 uptake and C_2H_4 productivity, these zeolites exhibit comparable or higher volumetric gas capacities along with lower adsorption enthalpy (table S3). Combined with their high selectivity, notable stability, and low cost, these zeolites are still placed among the best choices for this separation by far, especially from the point of view of practical application.

DISCUSSION

We have successfully proposed and demonstrated a strategy of engineering multiple fluorine binding sites in anion-pillared materials to maximize trace C_2H_2 capture for C_2H_4 purification. The resulting ZJU-300a features the unique multiple-site fluorine binding model, providing one of the strongest binding affinity to afford the benchmark C_2H_2 capture capacity at 0.01 bar. This material thus demonstrates a record high C_2H_2 uptake of 3.23 mmol g^{-1} (at 296 K and 0.01 bar) and one of the highest C_2H_2/C_2H_4 selectivity reported to date. The fundamental C_2H_2 binding and separation mechanisms have been illustrated by gas-loaded SCXRD studies. Breakthrough experiments on ZJU-300a revealed both unprecedented dynamic selectivity (264) and C_2H_4 productivity of 436.7 mmol g^{-1} for actual C_2H_2/C_2H_4 mixtures, far exceeding all the reported materials including SIFSIX-14-Cu-i (91 and 101.3 mmol g^{-1}) and Ni@FAU (97 and 116.8 mmol g^{-1}). Combined with its facile synthesis and ultrahigh water stability, this material represents by far the benchmark adsorbent for trace C_2H_2 removal from C_2H_2/C_2H_4 mixtures. This programmed gas binding engineering revealed in this work may provide some guidance to facilitate the design of ideal physisorbents with ultrahigh binding affinity for highly efficient capture of trace gas or volatile organic compounds.

MATERIALS AND METHODS

Chemicals

All raw chemicals and reagents were commercially available and used directly without further purification. TPE was simply synthesized through a multistep reaction procedure (fig. S1 and more details in the Supplementary Materials). N_2 (99.999%), C_2H_2 (99.6%), C_2H_4 (99.9%), He (99.999%), and mixed gases of C_2H_2/C_2H_4 = 1/99 (v/v) were purchased from JinGong Company (China).

Crystallization of $[Zn(TPE)SiF_6]_n$ (ZJU-300)

A solution of $ZnSiF_6{\cdot}6H_2O$ (0.518 mg, 0.0025 mmol) in 0.1 ml of methanol was added to a narrow glass tube. Methanol (2 ml) was carefully layered over this to act as a buffer layer. Last, a solution of TPE (1.01 mg, 0.003 mmol) in 0.3 ml of methanol was layered over the buffer layer, and the tube was left undisturbed for 1 week. Colorless block crystals of ZJU-300 were obtained.

Bulk synthesis of $[Zn(TPE)SiF_6]_n$ (ZJU-300)

ZJU-300 was synthesized by slowly mixing a methanol solution (5 ml) of $ZnSiF_6{\cdot}6H_2O$ (25.9 mg, 0.125 mmol) with a methanol solution (15 ml) of TPE (50.5 mg, 0.15 mmol) at 80°C in a 25-ml glass vial. The mixtures were then kept in an oven at 80°C for 10 min, followed by slowly cooling to room temperature. A white powder was obtained by filtration and washed with methanol.

Sample characterization

^{1}H nuclear magnetic resonance spectra were recorded on a Bruker Advance DMX500 spectrometer using tetramethylsilane as the internal standard. The PXRD patterns were measured in a range of 2θ = 2° to 45° on an X'Pert PRO diffractometer using a Cu-Kα (λ = 1.54184 Å) radiation source at room temperature. Thermogravimetric analysis was performed on a Netzsch TG209F3 instrument, and the sample was heated under N_2 atmosphere with a heating rate of 5 K min^{-1}. The SEM images were observed by Hitachi S-4800 field emission SEM.

Gas sorption measurements

Before the gas sorption test, the fresh sample was first solvent-exchanged with dry methanol at least eight times within 3 days to completely exchange the guest solvent molecules in the framework. The solvent-exchanged sample was evacuated at room temperature for 12 hours and further at 363 K for 12 hours until the outgas rate was 4 μmHg min^{-1} before measurements. Single-component gas adsorption isotherms of C_2H_2 and C_2H_4 were recorded by using a Micromeritics ASAP 2020 surface area analyzer, and a Julabo water bath was used to keep the adsorption tube at a constant temperature of 273, 283, 296, and 313 K, respectively. N_2 sorption isotherms were obtained on a Micromeritics ASAP 2460 instrument, and the sorption measurement was maintained at 77 K under liquid nitrogen bath. Kinetic sorption measurements were conducted by the Intelligent Gravimetric Analyzer (IGA001, Hiden, UK) under 296 K and 1 bar.

Single-crystal x-ray diffraction

SCXRD data were collected at 284 K for ZJU-300 and at 200 K for C_2H_2@ZJU-300a and C_2H_4@ZJU-300a on an Agilent Supernova charge-coupled device diffractometer equipped with graphite-monochromatic enhanced Mo-Kα radiation (λ = 0.71073 Å). A single crystal of solvent-exchanged ZJU-300 was selected and put into a capillary glass tube with inner diameter of 0.2 mm. This crystal was evacuated at 363 K for 12 hours, and the capillary glass tube was filled by pure C_2H_2 or C_2H_4 gas up to 1 bar and then sealed to obtain C_2H_2-loaded or C_2H_4-loaded ZJU-300a crystal. The datasets were corrected by empirical absorption correction using spherical harmonics, implemented in the SCALE3 ABSPACK scaling algorithm. The structure was solved by direct methods and refined by full-matrix least-squares methods with the SHELX-97 program package (*60*). The crystal data are summarized in table S1.

Breakthrough experiments

The breakthrough experiments were performed using a dynamic gas breakthrough apparatus equipped with stainless steel column (4.0 mm inner diameter by 120 mm). The mixed gas flows of C_2H_2/C_2H_4 (1/99, v/v) were introduced into breakthrough apparatus with the rate of 5 and 10 ml min^{-1} at 296 K and 1 bar, respectively. The weight of activated ZJU-300a sample packed in the column was 0.352 g. For comparison, the breakthrough experiments were further carried out in a packed column of activated SIFSIX-14-Cu-i/UTSA-200 (0.205 g) and SIFSIX-1-Cu (0.380 g) for 1/99 C_2H_2/C_2H_4 gas mixture under a total flow of 5 ml min^{-1} and ambient conditions, respectively. The outlet gas from the column was monitored using gas chromatography (GC-2014C, SHIMADZU) equipped with a thermal conductivity detector (detection limit, 0.1 ppm). The standard gas mixtures were detected to calibrate the concentration of the outlet gas. After every breakthrough experiment, the sample can be generated under a purging He gas with a flow of 10 ml min^{-1} at 363 K for 4 hours.

Supplementary Materials

This PDF file includes:

Supplementary Text
Figs. S1 to S32
Tables S1 to S5
References

REFERENCES AND NOTES

1. I. Amghizar, L. A. Vandewalle, K. M. Van Geem, G. B. Marin, New trends in olefin production. *Engineering* **3**, 171–178 (2017).
2. T. Ren, M. Patel, K. Blok, Olefins from conventional and heavy feedstocks: Energy use in steam cracking and alternative processes. *Energy* **31**, 425–451 (2006).
3. S. M. Sadrameli, Thermal/catalytic cracking of liquid hydrocarbons for the production of olefins: A state-of-the-art review II: Catalytic cracking review. *Fuel* **173**, 285–297 (2016).
4. H. Wang, Y. Liu, J. Li, Designer metal–organic frameworks for size-exclusion-based hydrocarbon separations: Progress and challenges. *Adv. Mater.* **32**, 2002603 (2020).
5. K. Adil, Y. Belmabkhout, R. S. Pillai, A. Cadiau, P. M. Bhatt, A. H. Assen, G. Maurin, M. Eddaoudi, Gas/vapour separation using ultra-microporous metal–Organic frameworks: Insights into the structure/separation relationship. *Chem. Soc. Rev.* **46**, 3402–3430 (2017).
6. R. E. Sikma, N. Katyal, S.-K. Lee, J. W. Fryer, C. G. Romero, S. K. Emslie, E. L. Taylor, V. M. Lynch, J.-S. Chang, G. Henkelman, S. M. Humphrey, Low-valent metal ions as MOF pillars: A new route toward stable and multifunctional MOFs. *J. Am. Chem. Soc.* **143**, 13710–13720 (2021).
7. X. Han, S. Yang, M. Schröder, Porous metal–organic frameworks as emerging sorbents for clean air. *Nat. Rev. Chem.* **3**, 108–118 (2019).
8. Y. Gu, J.-J. Zheng, K.-i. Otake, M. Shivanna, S. Sakaki, H. Yoshino, M. Ohba, S. Kawaguchi, Y. Wang, F. Li, S. Kitagawa, Host–guest interaction modulation in porous coordination polymers for inverse selective CO_2/C_2H_2 separation. *Angew. Chem. Int. Ed.* **60**, 11688–11694 (2021).
9. Z. Chen, K. O. Kirlikovali, P. Li, O. K. Farha, Reticular chemistry for highly porous metal–organic frameworks: The chemistry and applications. *Acc. Chem. Res.* **55**, 579–591 (2022).
10. X.-W. Zhang, D.-D. Zhou, J.-P. Zhang, Tuning the gating energy barrier of metal-organic framework for molecular sieving. *Chem* **7**, 1006–1019 (2021).
11. L. Li, L. Guo, D. H. Olson, S. Xian, Z. Zhang, Q. Yang, K. Wu, Y. Yang, Z. Bao, Q. Ren, J. Li, Discrimination of xylene isomers in a stacked coordination polymer. *Science* **377**, 335–339 (2022).
12. H. Yang, Y. Wang, R. Krishna, X. Jia, Y. Wang, A. N. Hong, C. Dang, H. E. Castillo, X. Bu, P. Feng, Pore-space-partition-enabled exceptional ethane uptake and ethane-selective ethane–-Ethylene separation. *J. Am. Chem. Soc.* **142**, 2222–2227 (2020).
13. Y.-S. Bae, C. Y. Lee, K. C. Kim, O. K. Farha, P. Nickias, J. T. Hupp, S. T. Nguyen, R. Q. Snurr, High propene/propane selectivity in isostructural metal–Organic frameworks with high densities of open metal sites. *Angew. Chem. Int. Ed.* **51**, 1857–1860 (2012).
14. H. Zeng, M. Xie, Y.-L. Huang, Y. Zhao, X.-J. Xie, J.-P. Bai, M.-Y. Wan, R. Krishna, W. Lu, D. Li, Induced fit of C_2H_2 in a flexible MOF through cooperative action of open metal sites. *Angew. Chem. Int. Ed.* **58**, 8515–8519 (2019).
15. T. He, X.-J. Kong, Z.-X. Bian, Y.-Z. Zhang, G.-R. Si, L.-H. Xie, X.-Q. Wu, H. Huang, Z. Chang, X.-H. Bu, M. J. Zaworotko, Z.-R. Nie, J.-R. Li, Trace removal of benzene vapour using double-walled metal–dipyrazolate frameworks. *Nat. Mater.* **21**, 689–695 (2022).
16. M. H. Mohamed, Y. Yang, L. Li, S. Zhang, J. P. Ruffley, A. G. Jarvi, S. Saxena, G. Veser, J. K. Johnson, N. L. Rosi, Designing open metal sites in metal–organic frameworks for paraffin/olefin separations. *J. Am. Chem. Soc.* **141**, 13003–13007 (2019).
17. J. Pang, F. Jiang, M. Wu, C. Liu, K. Su, W. Lu, D. Yuan, M. Hong, A porous metal-organic framework with ultrahigh acetylene uptake capacity under ambient conditions. *Nat. Commun.* **6**, 7575 (2015).
18. P.-Q. Liao, N.-Y. Huang, W.-X. Zhang, J.-P. Zhang, X.-M. Chen, Controlling guest conformation for efficient purification of butadiene. *Science* **356**, 1193–1196 (2017).
19. H. Zeng, M. Xie, T. Wang, R.-J. Wei, X.-J. Xie, Y. Zhao, W. Lu, D. Li, Orthogonal-array dynamic molecular sieving of propylene/propane mixtures. *Nature* **595**, 542–548 (2021).
20. Y.-Y. Xue, X.-Y. Bai, J. Zhang, Y. Wang, S.-N. Li, Y.-C. Jiang, M.-C. Hu, Q.-G. Zhai, Precise pore space partitions combined with high-density hydrogen-bonding acceptors within metal–

organic frameworks for highly efficient acetylene storage and separation. *Angew. Chem. Int. Ed.* **60**, 10122–10128 (2021).
21. Y. Ye, S. Xian, H. Cui, K. Tan, L. Gong, B. Liang, T. Pham, H. Pandey, R. Krishna, P. C. Lan, K. A. Forrest, B. Space, T. Thonhauser, J. Li, S. Ma, Metal-organic framework based hydrogen-bonding nanotrap for efficient acetylene storage and separation. *J. Am. Chem. Soc.* **144**, 1681–1689 (2022).
22. X. Han, S. Yang, Molecular mechanisms behind acetylene adsorption and selectivity in functional porous materials. *Angew. Chem. Int. Ed.* **62**, e202218274 (2023).
23. E. D. Bloch, W. L. Queen, R. Krishna, J. M. Zadrozny, C. M. Brown, J. R. Long, Hydrocarbon separations in a metal-organic framework with open iron(II) coordination sites. *Science* **335**, 1606–1610 (2012).
24. J. E. Bachman, M. T. Kapelewski, D. A. Reed, M. I. Gonzalez, J. R. Long, M_2(m-dobdc) (M = Mn, Fe, Co, Ni) metal–organic frameworks as highly selective, high-capacity adsorbents for olefin/paraffin separations. *J. Am. Chem. Soc.* **139**, 15363–15370 (2017).
25. S. Yang, A. J. Ramirez-Cuesta, R. Newby, V. Garcia-Sakai, P. Manuel, S. K. Callear, S. I. Campbell, C. C. Tang, M. Schröder, Supramolecular binding and separation of hydrocarbons within a functionalized porous metal–organic framework. *Nat. Chem.* **7**, 121–129 (2015).
26. T.-L. Hu, H. Wang, B. Li, R. Krishna, H. Wu, W. Zhou, Y. Zhao, Y. Han, X. Wang, W. Zhu, Z. Yao, S. Xiang, B. Chen, Microporous metal-organic framework with dual functionalities for highly efficient removal of acetylene from ethylene/acetylene mixtures. *Nat. Commun.* **6**, 7328 (2015).
27. J. Lee, C. Y. Chuah, J. Kim, Y. Kim, N. Ko, Y. Seo, K. Kim, T. H. Bae, E. Lee, Separation of acetylene from carbon dioxide and ethylene by a water-stable microporous metal–organic framework with aligned imidazolium groups inside the channels. *Angew. Chem. Int. Ed.* **57**, 7869–7873 (2018).
28. Y.-L. Peng, T. Pham, P. Li, T. Wang, Y. Chen, K.-J. Chen, K. A. Forrest, B. Space, P. Cheng, M. J. Zaworotko, Z. Zhang, Robust ultramicroporous metal–organic frameworks with benchmark affinity for acetylene. *Angew. Chem. Int. Ed.* **57**, 10971–10975 (2018).
29. O. T. Qazvini, R. Babarao, S. G. Telfer, Multipurpose metal–organic framework for the adsorption of acetylene: Ethylene purification and carbon dioxide removal. *Chem. Mater.* **31**, 4919–4926 (2019).
30. J. Li, L. Jiang, S. Chen, A. Kirchon, B. Li, Y. Li, H.-C. Zhou, Metal-organic framework containing planar metal-binding sites: Efficiently and cost-effectively enhancing the kinetic separation of C_2H_2/C_2H_4. *J. Am. Chem. Soc.* **141**, 3807–3811 (2019).
31. Z. Zhang, S. B. Peh, Y. Wang, C. Kang, W. Fan, D. Zhao, Efficient trapping of trace acetylene from ethylene in an ultramicroporous metal–organic framework: Synergistic effect of high-density open metal and electronegative sites. *Angew. Chem. Int. Ed.* **59**, 18927–18932 (2020).
32. Y. Chai, X. Han, W. Li, S. Liu, S. Yao, C. Wang, W. Shi, I. da-Silva, P. Manuel, Y. Cheng, L. D. Daemen, A. J. Ramirez-Cuesta, C. C. Tang, L. Jiang, S. Yang, N. Guan, L. Li, Control of zeolite pore interior for chemoselective alkyne/olefin separations. *Science* **368**, 1002–1006 (2020).
33. S. Dutta, S. Mukherjee, O. T. Qazvini, A. K. Gupta, S. Sharma, D. Mahato, R. Babarao, S. K. Ghosh, Three-in-one C_2H_2-selectivity-guided adsorptive separation across an isoreticular family of cationic square-lattice MOFs. *Angew. Chem. Int. Ed.* **61**, e202114132 (2022).
34. W. Fan, S. B. Peh, Z. Zhang, H. Yuan, Z. Yang, Y. Wang, K. Chai, D. Sun, D. Zhao, Tetrazole-functionalized zirconium metal-organic cages for efficient C_2H_2/C_2H_4 and C_2H_2/CO_2 separations. *Angew. Chem. Int. Ed.* **60**, 17338–17343 (2021).
35. S. Liu, Y. Chen, B. Yue, Y. Nie, Y. Chai, G. Wu, J. Li, X. Han, S. J. Day, S. P. Thompson, N. Guan, S. Yang, L. Li, Cascade adsorptive separation of light hydrocarbons by commercial zeolites. *J. Energy Chem.* **72**, 299–305 (2022).
36. J. Pei, K. Shao, J.-X. Wang, H.-M. Wen, Y. Yang, Y. Cui, R. Krishna, B. Li, G. Qian, A chemically stable Hofmann-type metal−organic framework with sandwich-like binding sites for benchmark acetylene capture. *Adv. Mater.* **32**, 1908275 (2020).
37. J. Wang, Y. Zhang, P. Zhang, J. Hu, R.-B. Lin, Q. Deng, Z. Zeng, H. Xing, S. Deng, B. Chen, Optimizing pore space for flexible-robust metal–organic framework to boost trace acetylene removal. *J. Am. Chem. Soc.* **142**, 9744–9751 (2020).
38. H. Li, C. Liu, C. Chen, Z. Di, D. Yuan, J. Pang, W. Wei, M. Wu, M. Hong, An unprecedented pillar-cage fluorinated hybrid porous framework with highly efficient acetylene storage and separation. *Angew. Chem. Int. Ed.* **60**, 7547–7552 (2021).
39. M. Shivanna, K.-i. Otake, B.-Q. Song, L. M. van Wyk, Q.-Y. Yang, N. Kumar, W. K. Feldmann, T. Pham, S. Suepaul, B. Space, L. J. Barbour, S. Kitagawa, M. J. Zaworotko, Benchmark acetylene binding affinity and separation through induced fit in a flexible hybrid ultramicroporous material. *Angew. Chem. Int. Ed.* **60**, 20383–20390 (2021).
40. J. Shen, X. He, T. Ke, R. Krishna, J. M. van Baten, R. Chen, Z. Bao, H. Xing, M. Dincă, Z. Zhang, Q. Yang, Q. Ren, Simultaneous interlayer and intralayer space control in two-dimensional metal–organic frameworks for acetylene/ethylene separation. *Nat. Commun.* **11**, 6259 (2020).
41. S. Noro, R. Kitaura, M. Kondo, S. Kitagawa, T. Ishii, H. Matsuzaka, M. Yamashita, Framework engineering by anions and porous functionalities of Cu(II)/4,4′-bpy coordination polymers. *J. Am. Chem. Soc.* **124**, 2568–2583 (2002).
42. P. Nugent, Y. Belmabkhout, S. D. Burd, A. J. Cairns, R. Luebke, K. Forrest, T. Pham, S. Ma, B. Space, L. Wojtas, M. Eddaoudi, M. J. Zaworotko, Porous materials with optimal adsorption thermodynamics and kinetics for CO_2 separation. *Nature* **495**, 80–84 (2013).
43. O. Shekhah, Y. Belmabkhout, Z. Chen, V. Guillerm, A. Cairns, K. Adil, M. Eddaoudi, Made-to-order metal-organic frameworks for trace carbon dioxide removal and air capture. *Nat. Commun.* **5**, 4228 (2014).
44. K.-J. Chen, H. S. Scott, D. G. Madden, T. Pham, A. Kumar, A. Bajpai, M. Lusi, K. A. Forrest, B. Space, J. J. Perry IV, M. J. Zaworotko, Benchmark C_2H_2/CO_2 and CO_2/C_2H_2 separation by two closely related hybrid ultramicroporous materials. *Chem* **1**, 753–765 (2016).
45. A. Cadiau, K. Adil, P. M. Bhatt, Y. Belmabkhout, M. Eddaoudi, A metal–organic framework-based splitter for separating propylene from propane. *Science* **353**, 137–140 (2016).
46. A. Cadiau, Y. Belmabkhout, K. Adil, P. M. Bhatt, R. S. Pillai, A. Shkurenko, C. Martineau-Corcos, G. Maurin, M. Eddaoudi, Hydrolytically stable fluorinated metal-organic frameworks for energy-efficient dehydration. *Science* **356**, 731–735 (2017).
47. X. Cui, K. Chen, H. Xing, Q. Yang, R. Krishna, Z. Bao, H. Wu, W. Zhou, X. Dong, Y. Han, B. Li, Q. Ren, M. J. Zaworotko, B. Chen, Pore chemistry and size control in hybrid porous materials for acetylene capture from ethylene. *Science* **353**, 141–144 (2016).
48. B. Li, X. Cui, D. O'Nolan, H.-M. Wen, M. Jiang, R. Krishna, H. Wu, R.-B. Lin, Y.-S. Chen, D. Yuan, H. Xing, W. Zhou, Q. Ren, G. Qian, M. J. Zaworotko, B. Chen, An ideal molecular sieve for acetylene removal from ethylene with record selectivity and productivity. *Adv. Mater.* **29**, 1704210 (2017).
49. Z. Zhang, X. Cui, L. Yang, J. Cui, Z. Bao, Q. Yang, H. Xing, Hexafluorogermanate (GeFSIX) anion-functionalized hybrid ultramicroporous materials for efficiently trapping acetylene from ethylene. *Ind. Eng. Chem. Res.* **57**, 7266–7274 (2018).
50. S. K. Elsaidi, M. H. Mohamed, T. Pham, T. Hussein, L. Wojtas, M. J. Zaworotko, B. Space, Crystal engineering of a 4,6-c fsc platform that can serve as a carbon dioxide single-molecule trap. *Cryst. Growth Des.* **16**, 1071–1080 (2016).
51. Q. Lin, C. Mao, A. Kong, X. Bu, X. Zhao, P. Feng, Porphyrinic coordination lattices with fluoropillars. *J. Mater. Chem. A* **5**, 21189–21195 (2017).
52. D. Sensharma, D. J. O'Hearn, A. Koochaki, A. A. Bezrukov, N. Kumar, B. H. Wilson, M. Vandichel, M. J. Zaworotko, The first sulfate-pillared hybrid ultramicroporous material, SOFOUR-1-Zn, and its acetylene capture properties. *Angew. Chem. Int. Ed.* **61**, e202116145 (2022).
53. P. Zhang, Y. Zhong, Y. Zhang, Z. Zhu, Y. Liu, Y. Su, J. Chen, S. Chen, Z. Zeng, H. Xing, S. Deng, J. Wang, Synergistic binding sites in a hybrid ultramicroporous material for one-step ethylene purification from ternary C_2 hydrocarbon mixtures. *Sci. Adv.* **8**, eabn9231 (2022).
54. Z. Niu, X. Cui, T. Pham, G. Verma, P. C. Lan, C. Shan, H. Xing, K. A. Forrest, S. Suepaul, B. Space, A. Nafady, A. M. Al-Enizi, S. Ma, A MOF-based ultra-strong acetylene nano-trap for highly efficient C_2H_2/CO_2 separation. *Angew. Chem. Int. Ed.* **60**, 5283–5288 (2021).
55. C. Y. Lee, Y.-S. Bae, N. C. Jeong, O. K. Farha, A. A. Sarjeant, C. L. Stern, P. Nickias, R. Q. Snurr, J. T. Hupp, S. T. Nguyen, Kinetic separation of propene and propane in metal organic frameworks: Controlling diffusion rates in plate-shaped crystals via tuning of pore apertures and crystallite aspect ratios. *J. Am. Chem. Soc.* **133**, 5228–5231 (2011).
56. A. L. Myers, J. M. Prausnitz, Thermodynamics of mixed-gas adsorption. *AIChE J.* **11**, 121–127 (1965).
57. A. Corma, E. Corresa, Y. Mathieu, L. Sauvanaud, S. Al-Bogami, M. S. Al-Ghrami, A. Bourane, Crude oil to chemicals: Light olefins from crude oil. *Cat. Sci. Technol.* **7**, 12–46 (2017).
58. D. O'Nolan, A. Kumar, M. J. Zaworotko, Water vapor sorption in hybrid pillared square grid materials. *J. Am. Chem. Soc.* **139**, 8508–8513 (2017).
59. M. Fakhroleslam, S. M. Sadrameli, Thermal/catalytic cracking of hydrocarbons for the production of olefins; a state-of-the-art review III: Process modeling and simulation. *Fuel* **252**, 553–566 (2019).
60. G. M. Sheldrick, SHELXL-97, Program for the Refinement of Crystal Structures (University of Göttingen, Göttingen, Germany 1997).

Acknowledgments
Funding: This research was supported by the National Science Foundation of China (52073251, 92163110, and U22A20251), the Zhejiang Provincial Natural Science Foundation of China (no. LR22E030003), and the Science Technology Department of Zhejiang Province (2022C01225).
Author contributions: X.-W.G. and E.W. synthesized and characterized the MOF samples and measured the adsorption isotherms. X.-W.G., E.W., and J.-X.W. collected and analyzed the SCXRD data. X.-W.G. and H.-M.W. measured and analyzed the breakthrough data. B.L., G.Q., and B.C. directed and supervised the project. B.L. wrote the paper, and all authors contributed to revising the manuscript. **Competing interests:** The authors declare that they have no competing interests. **Data and materials availability:** All data needed to evaluate the conclusions in the paper are present in the paper and/or the Supplementary Materials.

Crystallographic data for the structures in this article have been deposited at the Cambridge Crystallographic Data Centre under deposition nos. CCDC 2218592 (ZJU-300), 2218593 (C_2H_2@ZJU-300a), and 2218594 (C_2H_4@ZJU-300a). Copies of the data can be obtained free of charge from www.ccdc.cam.ac.uk/structures/.

Submitted 5 February 2023
Accepted 5 July 2023
Published 4 August 2023
10.1126/sciadv.adh0135